ROYAL SOCIETY OF CHEMISTRY

PAPER

Check for updates

Particle dispersion through porous media with heterogeneous attractions†

Wilfred Kwabena Darko, [ID][a] Deepak Mangal, [ID][b] Jacinta C. Conrad [ID][a] and Jeremy C. Palmer [ID] *[a]

Porous media used in many practical applications contain natural spatial variations in composition and surface charge that lead to heterogeneous physicochemical attractions between the media and transported particles. We performed Stokesian dynamics (SD) simulations to examine the effects of heterogeneous attractions on quiescent diffusion and hydrodynamic dispersion of particles within geometrically ordered arrays of nanoposts. We find that transport under quiescent conditions occurs by two mechanisms, diffusion through the void space and intermittent hopping between the attractive wells of different nanoposts. As the attraction heterogeneity increases, the latter mechanism becomes dominant, resulting in an increase in the particle trajectory tortuosity, deviations from Gaussian behavior in the particle displacement distributions, and a decrease in the long-time particle diffusivity. Similarly, under flow conditions corresponding to low Péclet number (Pe), increased attraction heterogeneity leads to transient localization near the nanoposts, resulting in a broadening of the particle distribution and enhanced longitudinal dispersion in the direction of flow. At high Pe where advection strongly dominates, however, the longitudinal dispersion coefficient is insensitive to attraction heterogeneity and exhibits Taylor–Aris dispersion behavior. Our findings provide insight into how heterogeneous interactions may influence particle transport in complex 3-D porous media.

1 Introduction

Particle dispersion within complex media is crucial for a wide range of practical applications, including separation processes like chromatography[1] and gel electrophoresis,[2] oil exploration and production,[3] and drug delivery.[4–6] These applications involve media composed of solids, fluid mixtures, and macromolecules. Particle transport in such heterogeneous environments is influenced by physicochemical and hydrodynamic interactions with the medium, as well as the coupling of particle dynamics with local[7,8] and cooperative[9–11] medium relaxations. Developing a fundamental understanding of these processes is vital to controlling particle transport through the wide variety of complex media encountered in practical settings.

Theoretical models[12–14] and simulation techniques[15–27] have been widely used to study particle transport at the pore scale. Whereas most of these studies have focused on the transport of infinitesimal tracers,[12,28–32] hydrodynamic and steric interactions with the medium can significantly affect the transport of particles whose diameter is on the same order as the characteristic pore size.[15,16,27,33–35] Moreover, non-steric physicochemical attractions, such as van der Waals and electrostatic forces, are prevalent in many applications but are often neglected. These interactions can lead to reversible and irreversible adsorption processes[36,37] that strongly influence the transport of tracer[25,26,38–40] and finite-sized particles.[27,41,42]

Although a large body of work exists on the effects of surface roughness and structural disorder on transport,[43–54] the influence of heterogeneous physicochemical attractions on particle diffusion and dispersion has received less attention. Heterogeneous physicochemical attractions are challenging to characterize experimentally,[55–57] but commonly arise in practical settings in which the transported particles and porous medium exhibit spatial variations in composition and surface charge.[55,58–64] Theoretical studies suggest that such variations can strongly influence the effective interactions between particle pairs and between particles and solid surfaces.[55,62,65–67] Additionally, they have been shown to influence transport properties near 2-D or quasi-2-D surfaces.[56,68,69] Nonetheless, the effects of heterogeneous interactions on the microscopic transport processes of particles through more complex 3-D porous media remain incompletely understood.

In this paper, we performed Stokesian dynamics (SD) simulations to examine the effects of heterogeneous attractive interactions between the particles and medium on quiescent diffusion and hydrodynamic dispersion within arrays of nanoposts, similar

[a] Department of Chemical and Biomolecular Engineering, University of Houston, Houston, Texas, 77204, USA. E-mail: jcpalmer@uh.edu
[b] Department of Mechanical and Industrial Engineering, Northeastern University, Boston, 02115, USA

to the geometrically ordered materials used in separation methods such as deterministic lateral displacement[70–74] and hydrodynamic chromatography.[75–77] Under quiescent conditions, transport is determined by the interplay between diffusion in the void space and intermittent hopping between the nanoposts. Increasing either the attraction well depth u_0 or heterogeneity β (the half-width of the well depth distribution) leads to slowing of diffusion on long time scales, as the hopping mechanism becomes dominant with the increase in the fraction of strongly attractive nanoposts. For moderate attractions, the particle displacement distributions become increasingly non-Gaussian and the particle trajectories become more tortuous as β increases. Under flow conditions, transport is determined by the interplay between thermal fluctuations, attractive particle–nanopost interactions, and advective drag forces. Moderate attractions drive transient localization near the nanoposts, which broadens the distribution of particles and, thereby, increases longitudinal dispersion at low Péclet (Pe) number. This effect strengthens as heterogeneity increases. At high Pe, however, advection dominates and longitudinal dispersion is independent of β. Finally, we show that heterogeneity in the strength of attractions does not strongly affect directional locking behavior. Our findings provide insight into how heterogeneous composition or surface charge may influence particle transport in complex 3-D porous media.

2 Methods

We used SD to simulate the transport of particles (P) through three-dimensional arrays of nanoposts (NP) with heterogeneous attractions. Simulations were performed and analyzed using d_p, $k_B T$, and $\tau_d = 3\pi\eta d_p^3/4k_B T$ as characteristic units for length, energy, and time, respectively. Here, d_p is the particle diameter, k_B is the Boltzmann constant, T is temperature, τ_d is the diffusive time scale, and η is the dynamic fluid viscosity.

Following our previous studies,[35,42,78] each nanopost was modeled as an immobile chain of 20 spherical beads of diameter $d_{np} = d_p$. The arrays consisted of 100×100 nanoposts placed on a regular square lattice in the x–y plane of the simulation cell with their major axes aligned along the z direction (Fig. 1). Accordingly, the solid volume fraction is given by $\phi = \pi d_{np}^2/6L^2$, where L is the spacing between adjacent posts.

Particle–nanopost interactions were modeled using the Yukawa potential with a repulsive, hard-sphere core:[27]

$$u(r_{ij}) = \begin{cases} -u_{0,j}\exp(-\kappa r_{ij}), & r_{ij} \geq 0 \\ \infty, & r_{ij} < 0 \end{cases} \quad (1)$$

where $u_{0,j}$ and κ are the depth and range of the attraction well, and r_{ij} is the surface-to-surface distance between the particle i and nanopost j. Heterogeneity in the particle–nanopost interactions was introduced into the system by assigning a random well depth $u_{0,j}$ to each nanopost drawn from a uniform distribution $u_0 \mathscr{U}(1 - \beta, 1 +\beta)$, where $u_0 = \langle u_{0,j}\rangle$ is the mean well depth and β is the half-width of the distribution (Fig. S1 and S2 in ESI†). We investigated systems with $\kappa = 30$ and u_0 in the
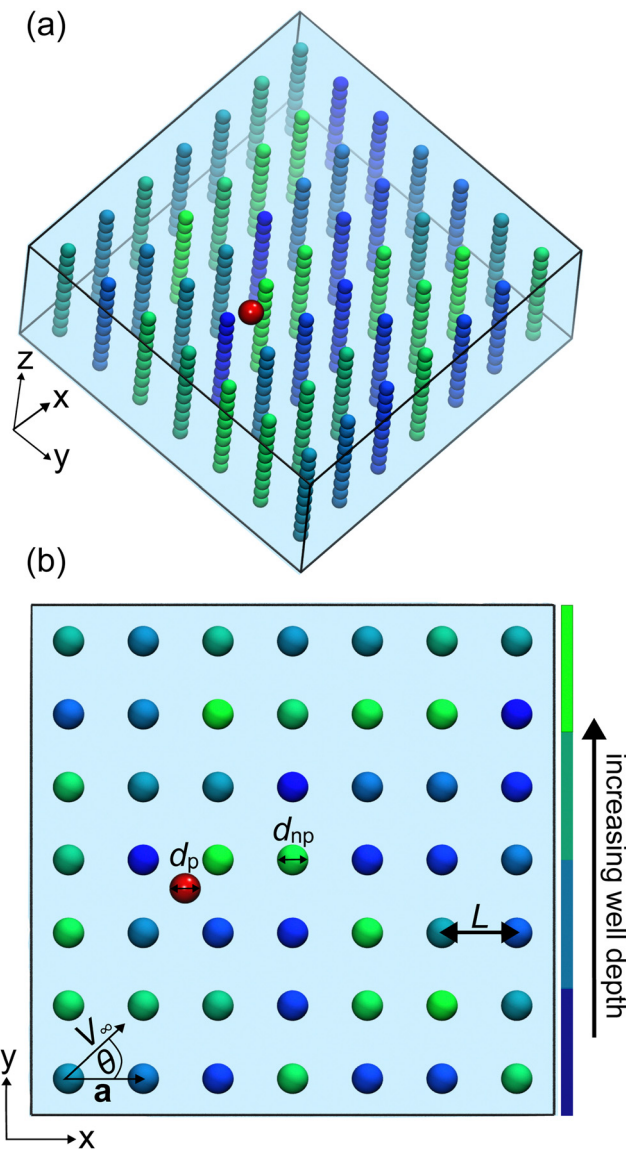

Fig. 1 Schematic illustrations of a 7×7 subsection of the 100×100 nanopost arrays. (a) A three-dimensional perspective view of the array subsection. (b) A two-dimensional orthographic projection of the array subsection in the x–y plane. The nanoposts are colored using a blue-to-green scheme to indicate increasing well depth $u_{0,j}$. The transported particle (red) is the same size as the spheres in the NPs (i.e., $d_p = d_{np}$). L is the lattice spacing (center-to-center spacing between adjacent posts), and θ is the angle of the incident flow relative to the lattice vector a.

range 0–7, yielding interactions typical of those for particles in porous media.[42,59,79] Additionally, to prevent the Yukawa potential from being repulsive for $r_{ij} \geq 0$, we only consider $\beta \leq u_0$.

The simulations were conducted under dilute conditions by considering the transport of a single particle through the nanopost arrays. Both short- and long-range hydrodynamic interactions were modeled, using the Ewald summation method to accurately treat the latter,[27,80–82] and periodic boundary conditions were applied along all three dimensions of the simulation cell. Flow through the arrays was driven by

imposing a uniform suspension velocity $\mathbf{V}_\infty$ with orientation $\theta = \arccos\left(\dfrac{\mathbf{V}_\infty \cdot \mathbf{a}}{|\mathbf{V}_\infty||\mathbf{a}|}\right)$ relative to the lattice vector $\mathbf{a}$ (Fig. 1(b)). Depending on u_0 and $V_\infty = |\mathbf{V}_\infty|$, the equations of motion were integrated using a time step dt in the range 5×10^{-6}–5×10^{-5}, and the simulations were run for a total duration of 1×10^4–2×10^6 time units (2×10^9–4×10^{10} time steps). Other details of SD simulations are identical to those in our previous studies.[35,42,78]

Transport properties were determined by averaging over approximately 100 independent particle trajectories. Under quiescent conditions (*i.e.*, $V_\infty = 0$), the particle diffusivity was extracted from the long-time limit of the ensemble-averaged, three-dimensional mean-squared displacement (MSD), $D_q = \lim_{t \to \infty} \frac{1}{6}\mathrm{d}\langle \Delta r^2(t) \rangle / \mathrm{d}t$. Under flow conditions, the asymptotic longitudinal dispersion coefficient (dispersion in the direction of flow) D_L was evaluated via:[30,83]

$$D_L \equiv \lim_{t \to \infty} \frac{1}{2} \frac{\mathrm{d}\sigma_L^2(t)}{\mathrm{d}t}, \qquad (2)$$

where $\sigma_L^2(t) = \langle (\Delta r_L(t) - \langle V_L \rangle t)^2 \rangle$ is the particle MSD evaluated in the frame of reference of the average longitudinal velocity $\langle V_L \rangle$, which was estimated from a linear fit to the average particle displacements over time. The diffusivity of a freely-diffusive particle $D_0 = k_B T / 3\pi \eta d_p$ was used to normalize D_q and D_L.

3 Results and discussion

3.1 Quiescent diffusion

We first examined how the particle MSDs are affected by the attraction strength (u_0) and heterogeneity (β). For weak attractions ($u_0 = 3$), the MSDs exhibit $\langle \Delta r^2(t) \rangle \sim t^1$ scaling over the full range of time scales examined and vary little with β, indicating that the attractions with the nanoposts are too weak to significantly hinder diffusion (Fig. 2(a)). Similar behavior is observed for systems with strong attraction strengths ($u_0 = 7$) and low heterogeneity ($\beta < 2$). As β increases, however, we observe the appearance of a crossover at $t \approx 10^1 - 10^2$ to a second diffusive regime at long times characterized by significantly slower dynamics (Fig. 2(b) and Fig. S3 in ESI†). This crossover behavior reflects the interplay between two transport mechanisms: diffusion through the void space and intermittent hopping between the attractive wells of different nanoposts (Movies S1 and S2 in ESI†). The former is a rapid process that is dominant on all time scales in arrays with weak attractions. For systems with moderate and strong attractions, it is also dominant on short times scales on which particles are unlikely to become localized in the attractive wells surrounding the nanoposts. Accordingly, as u_0 and β increase, the characteristic time scale of the crossover decreases due to the increased prevalence of nanoposts with highly attractive wells. By contrast, the latter mechanism results in a slower diffusive process that becomes increasingly dominant on long time scales as the fraction of highly attractive nanoposts increases.

The normalized asymptotic diffusivity D_q/D_0 is strongly influenced by the interplay between these two diffusive
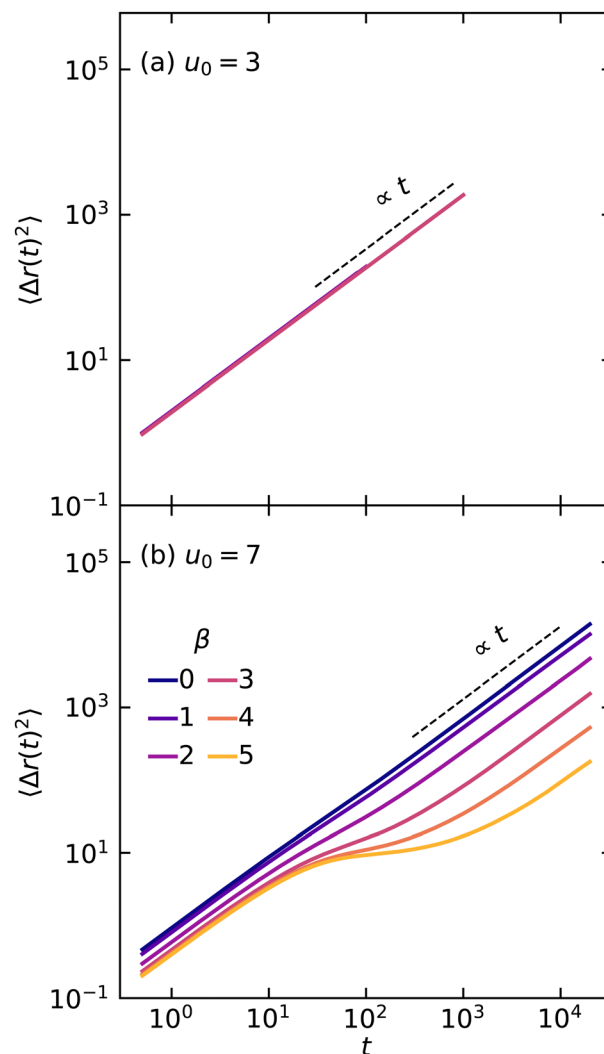

Fig. 2 Particle mean-squared displacements $\langle \Delta r^2(t) \rangle$ as functions of lag time t in nanopost arrays with $\phi = 0.014$ and $u_0 = $ (a) 3 and (b) 7. The dashed lines are references indicating $\propto t$ scaling. The legend in (b) applies to both panels.

mechanisms on long times as u_0 and β are varied. As shown in ref. 42, in the case of purely repulsive interactions ($u_0 = 0$), the diffusive behavior is well described by a hydrodynamic theory for hindered diffusion.[84] For $u_0 = 3$ and $\beta = 0$, D_q/D_0 is approximately equal to that for the repulsive case, indicating that thermal fluctuations allow the particles to readily escape the weakly attractive regions surrounding the nanoposts (Fig. 3(a)). As β increases, D_q/D_0 slowly decreases and departs from the limiting vale for $u_0 = 0$. For $u_0 = 5$, D_q/D_0 is significantly lower than the limiting value for $u_0 = 0$ even when $\beta = 0$, and it decreases more rapidly with increasing β than in the case for $u_0 = 3$ (Fig. 3(a)). The sharp decrease in D_q/D_0 at large u_0 is consistent with previous investigations of porous media with homogeneous attractions (*i.e.*, $\beta = 0$), including a theoretical model[85] and simulations of particle transport in nanopost arrays[42] and hydrogel matrices.[27] Interestingly, in contrast with the decrease in D_q/D_0 upon increasing β, experiments on similar

nanopost arrays suggest increasing structural heterogeneity produces large void spaces that enhance the overall particle diffusivity.[51] Upon further increasing the well depth to $u_0 = 7$, the normalized diffusivity exhibits a precipitous drop at low β (Fig. 3(a)). The decrease in D_q/D_0 with β for $u_0 = 7$ is less pronounced than for the case of $u_0 = 5$, and the normalized diffusivity appears to eventually saturate at a low value at high β, indicating that the hopping diffusion mechanism is dominant. Thus, the effects of attraction heterogeneity (β) on diffusion are most pronounced at intermediate u_0 where the particle–nanopost interactions begin to compete with thermal fluctuations, resulting in two diffusion mechanisms. Due to enhanced confinement, the diffusivity decreases as the nanopost volume fraction ϕ is increased (Fig. 3(b) and Fig. S4 in ESI†). Nevertheless, the trends observed upon changing u_0 or β remain qualitatively similar for all values of ϕ investigated.

These two diffusion mechanisms also result in qualitatively different particle displacement distributions. In the presence of weak attractions ($u_0 = 3$), the particle displacement distribution $p(\Delta x)$ is Gaussian, as is typical for normal diffusion (Fig. S5(a) in ESI†). Whereas Gaussian behavior is still observed for moderate attractions ($u_0 = 5$) and $\beta = 0$, the distribution $p(\Delta x)$ becomes increasingly non-Gaussian as β increases (Fig. 4). This non-Gaussian behavior manifests itself on both the short ($t = 5$) (Fig. 4(a)) and long ($t = 10^3$) (Fig. 4(b)) time scales relevant to the early and asymptotic diffusive regimes in the MSDs, respectively. Hence, although the hopping mechanism is not dominant on short time scales, transient localization around the nanoposts results in anomalous diffusion in which the MSDs scale $\propto t$ but the displacement distributions deviate from normal Gaussian behavior. Similar behavior has been reported in structurally disordered nanopost arrays, where it was attributed to the spatially heterogeneous particle distributions and local dynamics.[51] The localization of particles around highly attractive nanoposts, which are randomly distributed throughout the arrays, has similar effects on the particle distribution and local dynamics and thus also produces non-Gaussian behavior.

Lastly, we characterize the effects of u_0 and β on the tortuosity of the particle trajectories:[35]

$$\langle \tau \rangle = \lim_{k \to \infty} \langle \tau_k \rangle = \lim_{k \to \infty} \left\langle \sum_{i=1}^{k} \frac{L_i}{\Delta L_k} \right\rangle \quad (3)$$

where L_i and ΔL_k are the linear distances between points along the trajectory separated by time intervals δt and $k\delta t$, respectively, and $\langle \cdots \rangle$ denotes the average over the ensemble of particle trajectories. For $u_0 = 3$, β has little effect on the tortuosity of the particle trajectories, consistent with the relatively small change in diffusivity observed under these conditions (Fig. 5 and Fig. S6 in ESI†). By contrast, for $u_0 = 5$, $\langle \tau \rangle$ is initially independent of β and then increases for $\beta \geq 2$. For $u_0 = 7$, $\langle \tau \rangle$ exhibits similar behavior; however, its rate of increase decreases at sufficiently high β as the hopping diffusion mechanism becomes dominant in this regime. Thus, these results show that transient localization in the attractive wells around the nanoposts significantly increases the diffusion path length through the nanopost arrays, resulting in a concomitant decrease in the particle diffusivity and slowing of the overall dynamics.

3.2 Transport under flow

We investigated the effects of attraction heterogeneity on particle transport under flow by imposing a uniform suspension velocity $\mathbf{V}_\infty$ oriented at an angle of $\theta = 45°$ with respect to the lattice vector $\mathbf{a}$. The spreading of particles in the direction of flow was characterized by computing the normalized longitudinal dispersion coefficient D_L/D_0 as a function of the Péclet number Pe $= \langle V_L \rangle d_p / D_0$, the dimensionless ratio of the rate of advection to the rate of diffusion. Imposed suspension
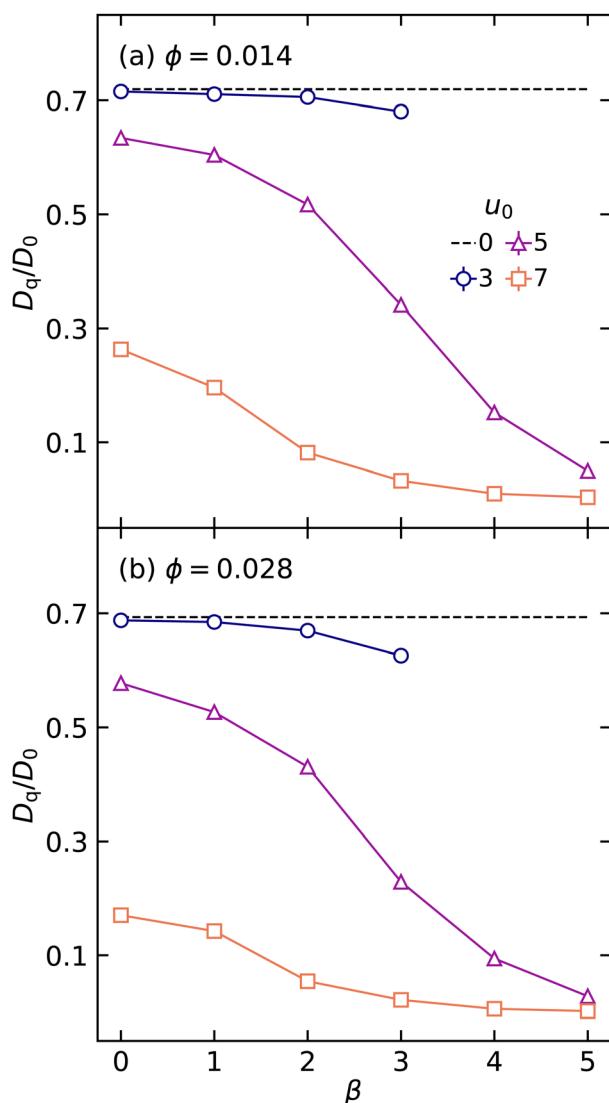

Fig. 3 Normalized diffusion coefficients D_q/D_0 as functions of the heterogeneity parameter β in nanopost arrays with ϕ = (a) 0.014 and (b) 0.028. The dashed lines indicate the values of D_q/D_0 for cases where $u_0 = 0$. The legend in (a) applies to both panels. Estimated uncertainties are smaller than the symbol sizes.
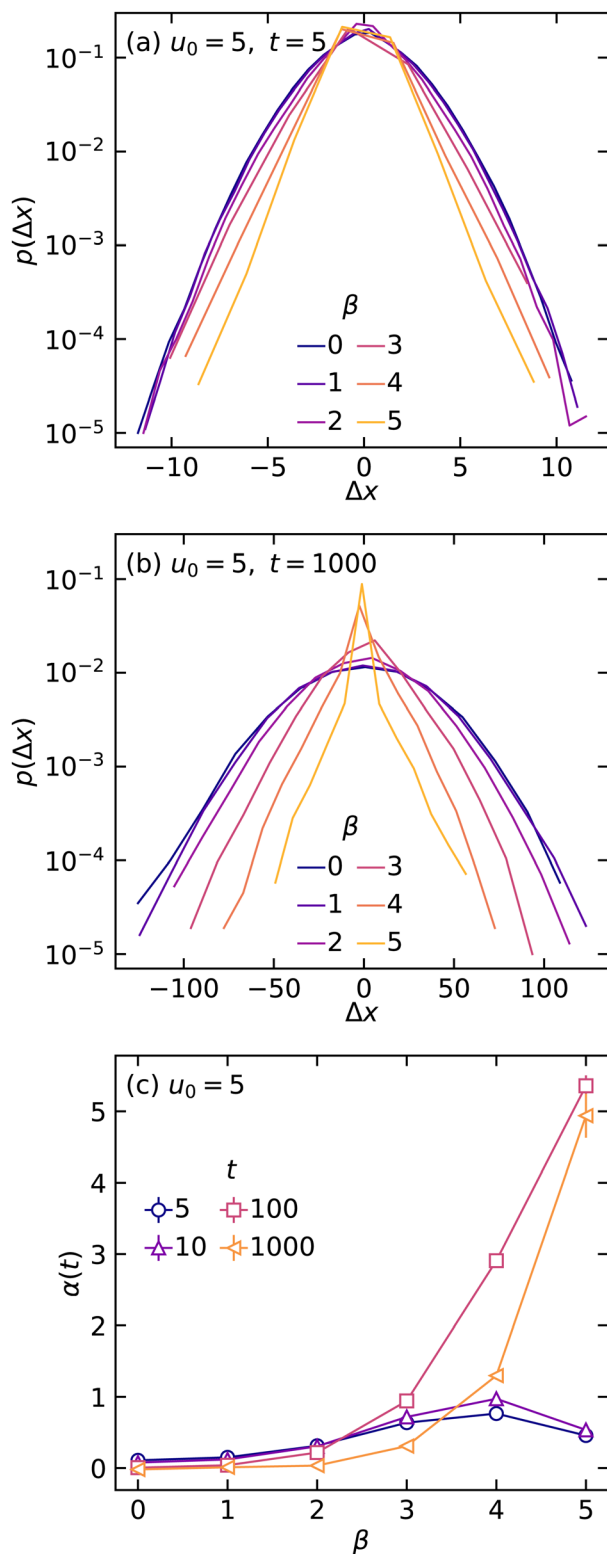
Fig. 4 Particle displacement distributions for nanopost arrays with $\phi = 0.028$ and $u_0 = 5$ at different lag times $t =$ (a) 5 and (b) 1000. The lag times are chosen to lie within the different diffusive regimes observed in the corresponding MSDs. The legend in (b) applies to (a) also. (c) Non-Gaussian parameters $\alpha(t) = \frac{1}{3} \langle \Delta x^4(t) \rangle \langle \Delta x^2(t) \rangle^{-2} - 1$ for the particle displacement distributions $p(\Delta x)$ calculated as functions of the heterogeneity parameter β at lag times of $t = 5, 10, 100,$ and 1000.
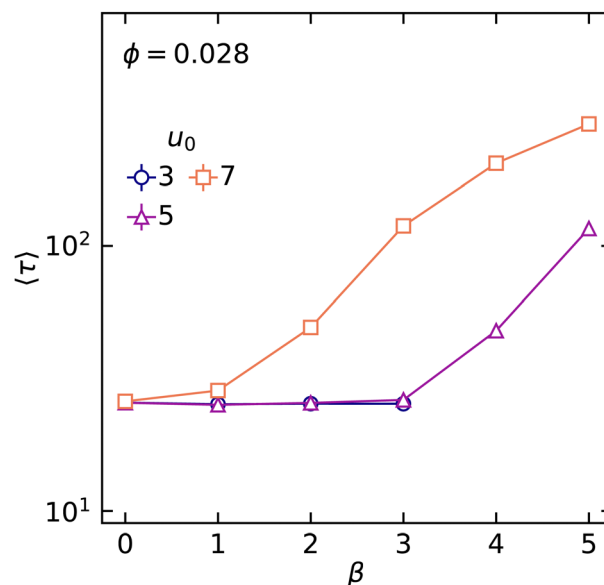

Fig. 5 Tortuosities $\langle \tau \rangle$ as functions of the heterogeneity parameter β for $u_0 = 3, 5,$ and 7 in nanopost arrays of $\phi = 0.028$. Estimated uncertainties are smaller than the symbol sizes.

velocities $V_\infty = 0$–1000 resulted in Pe = 0–10^3, covering the range accessible in experiment and relevant to probing regimes dominated by different transport mechanisms.[71,78,80,86] In the absence of attractions ($u_0 = 0$), D_L/D_0 increases gradually with Pe for $10^0 \leq$ Pe $\leq 10^1$ (Fig. 6). At large Pe (Pe $\geq 10^1$), where advective transport is dominant, D_L/D_0 increases rapidly and eventually crosses over to Pe^n scaling with $n \approx 2$, as predicted for Taylor–Aris dispersion.[12,78,87] Longitudinal dispersion is increasingly enhanced for Pe $\geq 10^1$ as the attraction strength u_0 is increased. For systems with low heterogeneity ($\beta \leq 2$), the increase in D_L/D_0 is relatively uniform for Pe $\geq 10^1$. As β increases, the asymptotic dispersion behavior at high Pe remains largely unchanged, but D_L/D_0 increases significantly at low Pe. Similar qualitative trends are observed when the particle–nanopost attraction strength has a log-normal rather than a uniform distribution (Fig. S7 in ESI†). This behavior reflects a complex interplay between advective transport and the two diffusion mechanisms. At low Pe, where transport is dominated by diffusion, increasing u_0 and/or β results in attractions with the nanoposts that are sufficiently strong to overcome thermal fluctuations. These attractions lead to enhanced particle localization, which broadens the distribution and increases dispersion in the direction of flow. By contrast, in the advection-dominated regime at high Pe, the viscous drag force on the particles is larger than those arising from particle–nanopost interactions or thermal fluctuations, and hence dispersion is largely unaffected by modest changes in u_0 and/or β.

Computational studies of passive tracer particles in disordered media predict a crossover from $n = 2$ to $n = 1$ scaling at high Pe as the degree of structural heterogeneity is increased.[86] Whereas the $n = 2$ scaling is associated with molecular diffusion, the $n = 1$ behavior is associated with mechanical dispersion arising from heterogeneity of the locally averaged fluid
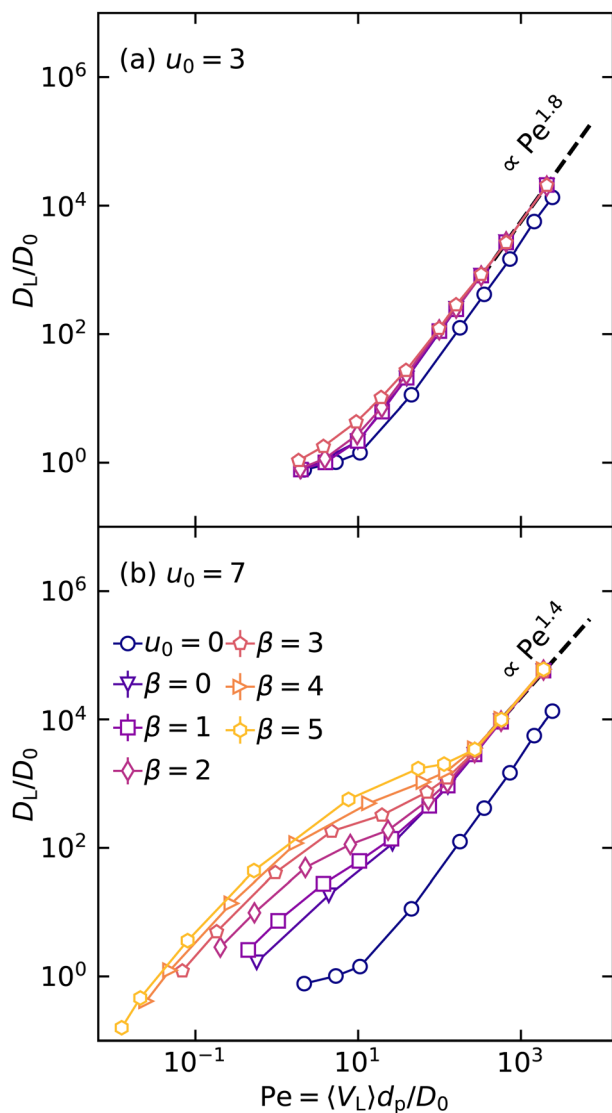
Fig. 6 Normalized longitudinal dispersion coefficients D_L/D_0 as functions of Pe for nanopost arrays with $\phi = 0.028$ and $u_0 = $ (a) 3 and (b) 7. The legend in (b) applies to both panels. The dashed lines are linear fits at high Pe. Estimated uncertainties are smaller than the symbol sizes.
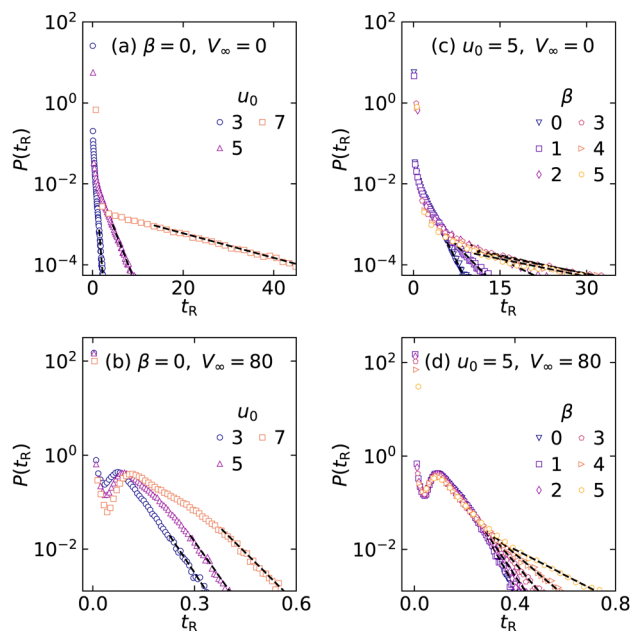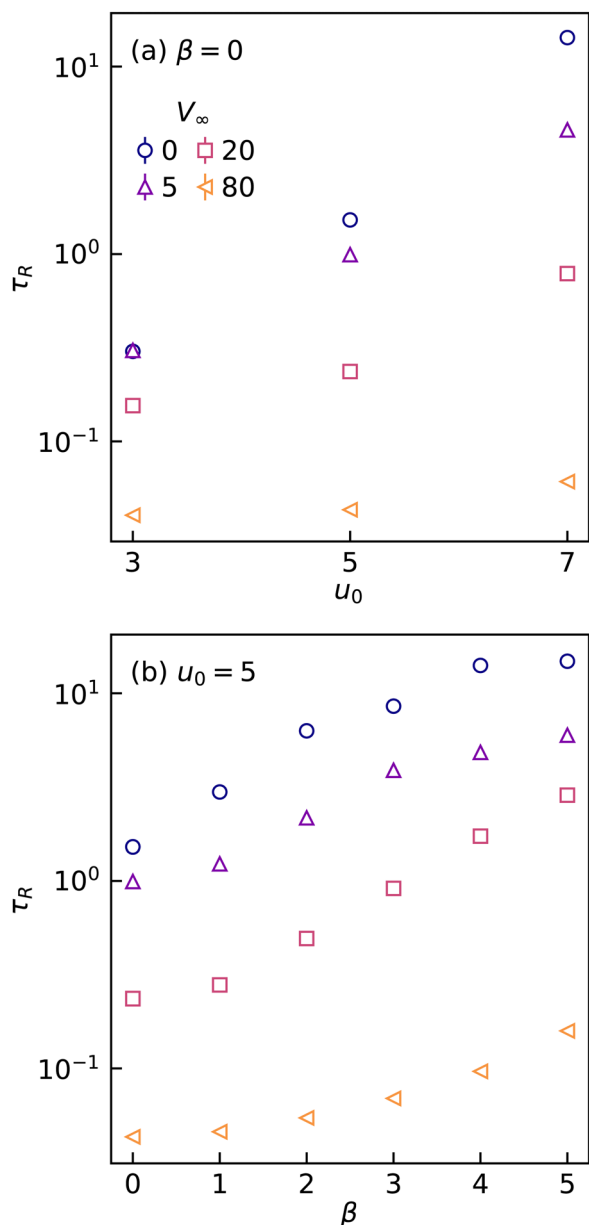

Fig. 7 Particle residence time distributions $P(t_R)$ at flow rates $V_\infty = $ (a), (c) 0 and (b), (d) 80 for nanopost arrays with $\phi = 0.028$. Panels (a) and (b) show distributions for homogeneous arrays ($\beta = 0$) as functions of well depth u_0, whereas panels (c) and (d) show distributions for heterogeneous arrays ($\beta > 0$) with $u_0 = 5$ as functions of β. The dashed black lines are fits of the exponential tail regions to $P(t_R) = c\exp^{-t_R/\tau_R}$, where c is a fitting constant.

velocity field.[12,86] Although we observe that n decreases slightly with increasing attraction strength u_0, the scaling for a given u_0 is relatively insensitive to β. Thus, no such crossover with β is observed for our systems because increasing the attraction heterogeneity does not affect the fluid velocity field.

The degree of localization was quantified by computing the particle residence time distribution $P(t_R)$, where t_R is the duration spent within a thin shell around the nanoposts. To encompass the attractive well around each nanopost, a shell width of 0.1 based on the particle–nanopost surface-to-surface distance was used in evaluating t_R. In the absence of flow ($V_\infty = 0$), the residence time distribution $P(t_R)$ exhibits a pronounced initial decrease arising from local Brownian motions that cause particles near the boundaries to fluctuate in and out of the shell regions (Fig. 7). For homogeneous systems ($\beta = 0$), this initial decrease is followed by a sharp

crossover to exponential decay at large t_R. As u_0 increases, the width of the exponential tail increases, but the crossover remains relatively sharp. Although increasing β also widens the $P(t_R)$ distributions, it broadens the crossover region and shifts the exponential decay to larger t_R. The broadening of the crossover region is due to the superposition of different localization processes with different characteristic t_R associated with the heterogeneous distribution of particle–nanopost interactions. The eventual crossover to exponential decay at large t_R in these heterogeneous systems indicates that this region is dominated by a single process associated with localization near the most strongly attractive nanoposts. Under flow ($V_\infty = 80$), $P(t_R)$ also exhibits a pronounced initial decrease and exponential tail at small and large t_R, respectively. At intermediate t_R, however, $P(t_R)$ exhibits a local maximum associated with trajectories in which particles advect along flow streamlines through the shell regions around the nanoposts.

We estimated the characteristic residence time τ_R associated with the exponential tail of the residence time distributions by fitting this region to $P^{\text{fit}}(t_R) = ce^{-t_R/\tau_R}$, where c is a fitting constant.[25,88] Previous studies have demonstrated that dispersion behavior is strongly correlated with τ_R.[25,26] For the homogeneous systems ($\beta = 0$), we observe that τ_R increases exponentially with u_0 for all flow rates examined (Fig. 8). Similar exponential increases in τ_R with u_0 have been observed in computational studies of polymer transport in nanopost arrays[88] and across surfaces.[89] This behavior is also in accord with the Frenkel model, which predicts that the average residence time will increase exponentially with adsorption strength

Fig. 8 Characteristic particle residence times τ_R for nanopost arrays with $\phi = 0.028$ obtained from fitting the exponential tail regions of the $P(t_R)$ distributions. Panel (a) shows τ_R for homogeneous arrays ($\beta = 0$) as functions of well depth u_0, whereas panel (b) shows τ_R for heterogeneous arrays ($\beta > 0$) with $u_0 = 5$ as functions of β. The legend in (a) applies to both panels. Estimated uncertainties are smaller than the symbol sizes.

for a first-order desorption process.[26,90,91] Although τ_R also increases with β, the growth deviates from exponential behavior. These deviations indicate that the tail regions of $P(t_R)$ for these heterogeneous systems may be influenced by competing localization processes, despite their apparent exponential decay with increasing t_R.

The interplay between advective drag forces, thermal fluctuations, and attractive interactions can be visually observed by inspecting the log-probability density distribution of the particle positions in the x–y plane $\log_{10}P(x, y)$ (Fig. S8 in ESI†). At

low flow rate ($V_\infty = 10$) and moderate interaction strength ($u_0 = 5$), increasing β leads to an increase in particle localization around highly attractive nanoposts and a greater degree of heterogeneity in the density distributions. As the flow rate is increased, however, the advective drag forces become increasingly dominant, resulting in more uniform sampling of the void space, except in regions of wake behind the nanoposts along the direction of flow. These changes are also reflected in the average tortuosity $\langle \tau \rangle$ of the particle trajectories (Fig. 9 and Fig. S9 and S10 in ESI†). At low Pe (<0.05; low V_∞), increasing the fraction of highly attractive nanoposts (by increasing u_0 and/or β) results in the hopping mechanism becoming dominant and more tortuous trajectories characterized by larger $\langle \tau \rangle$, similar to the behavior observed under quiescent conditions. At Pe ≈ 0.08, $\langle \tau \rangle$ exhibits a sharp decrease, indicating an abrupt transition from transport *via* hopping to an advection dominated mechanism where particles move along streamlines through the nanopost array. Further increases in Pe beyond this threshold value results in a gradual decay in $\langle \tau \rangle$ as it approaches its asymptotic value of unity as Pe $\rightarrow \infty$.

Lastly, we examine the influence of attraction heterogeneity on the phenomenon of directional locking. In our previous study of particle transport in square and hexagonal arrays with repulsive, non-hydrodynamic particle–nanopost interactions (*i.e.*, $u_0 = 0$), we observed a pronounced reduction in mean particle velocity and longitudinal dispersion for flow orientations slightly offset from the primitive lattice vectors.[78] This reduction was caused by directional locking, where steric interactions with the nanoposts lead to particle dynamics dominated by advection along a specific vector across a range of θ.[23] In the context of practical applications, this phenomenon can be exploited in deterministic lateral displacement
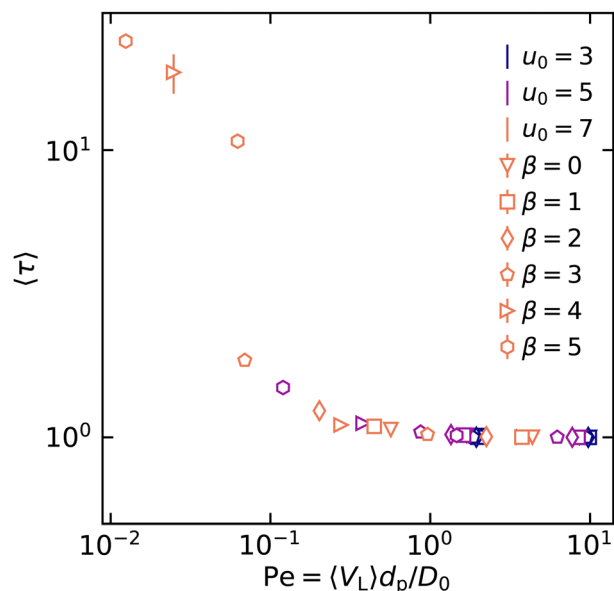
Fig. 9 Tortuosities $\langle \tau \rangle$ as functions of Pe in nanopost arrays with $\phi = 0.028$ for all u_0 and β studied. The symbols and colors denote different values of β and u_0, respectively.
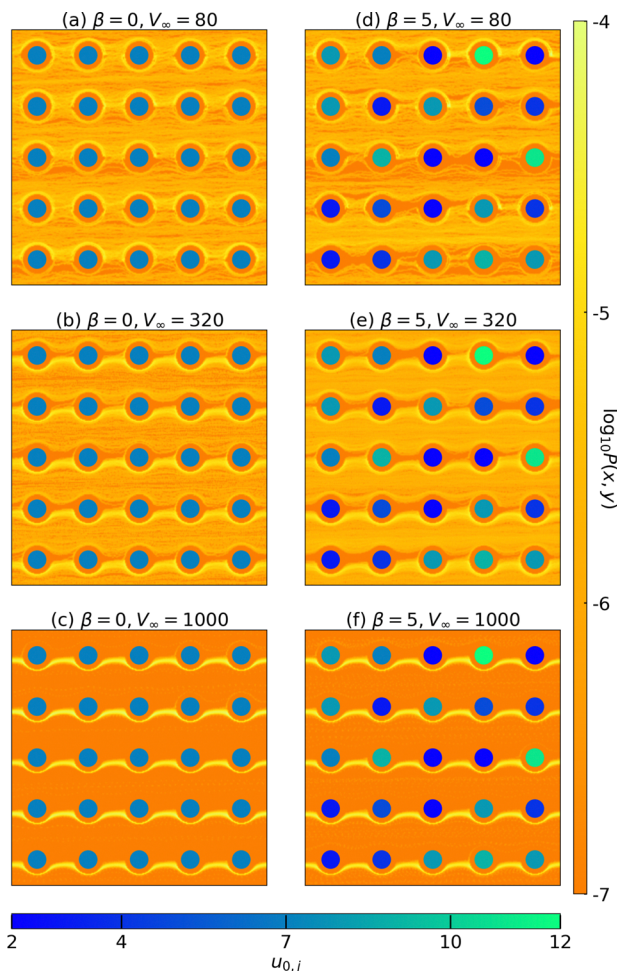
Fig. 10 Log-probability density distributions of particle positions $\log_{10} P(x, y)$ at flow rates V_∞ = (a), (d) 80, (b), (e) 320 and (c), (f) 1000 and orientation θ = 1.25° in 5 × 5 subsections of nanopost arrays with ϕ = 0.058, u_0 = 7, and heterogeneity parameter β = (a)–(c) 0 and (d)–(f) 5. The nanoposts are colored using a blue-to-green scheme to indicate increasing well depth $u_{0,j}$.

Fig. 11 Normalized longitudinal dispersion coefficients D_L/D_0 as functions of flow orientation θ for nanopost arrays with ϕ = 0.058 at u_0 = 7 when (a) β = 0 and (b) β = 5. The legend in (a) applies to both panels. Estimated uncertainties are smaller than the symbol sizes.

devices to sort particles by size.[23,92] It has also attracted attention as a route to separate particles driven through periodic potential fields.[13,14,17,18,20,21,24]

For square nanopost arrays, directional locking is most pronounced for flow orientations slightly perturbed from θ = 0° (*i.e.*, slightly misaligned from the primitive lattice vector **a**).[78] Thus, we examined this behavior at a flow orientation of 1.25°. Consistent with our previous study,[42] log-probability density distributions of the particle positions reveal that directional locking in homogeneous systems (β = 0) with attraction strength u_0 = 7 is only observed at high flow rates (V_∞ = 1000) (Fig. 10). Indeed, the particle distributions become increasingly narrow as V_∞ increases, reflecting the onset of directional locking (Fig. 10(a)–(c)). Relative to repulsive systems (u_0 = 0),[78] the onset of this behavior is observed at larger V_∞, demonstrating that attractive interactions compete with advective and steric forces to frustrate directional locking. At low flow rates, the attractions are sufficiently strong to drive particles to
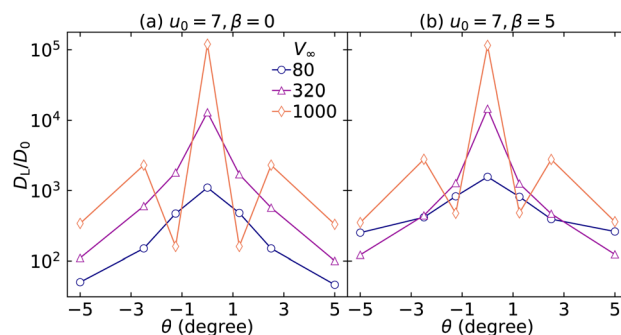
the regions of wake behind the nanoposts, where they are then transported along flow streamlines that lead to the upper hemisphere of the next nanopost (Fig. 10(a)). Thus, particles are able to transport in the direction perpendicular to the incident flow under these conditions. At high flow rates, however, the attractions are overcome by strong advective forces and the particles remain nearly perfectly locked along the vector **a** due to frequent collisions with the nanoposts (Fig. 10(c)). For systems with heterogeneous attractions (β = 5), the particle distributions exhibit larger variations at low flow rates (Fig. 10(d)). Nonetheless, similar to the case for systems with homogeneous attractions, near perfect directional locking is observed as advective forces become dominant at high V_∞ (Fig. 10(f)).

In agreement with the particle position distributions, we observe that the variations in the normalized longitudinal dispersion coefficient D_L/D_0 with flow orientation and rate are qualitatively similar in nanopost arrays with homogeneous and heterogeneous attractions (Fig. 11). At low flow rates, the dispersion coefficient exhibits a maximum at θ = 0° and gradually decreases as θ is varied from this value due to the ability of the particle to sample all streamlines under these conditions. At high flow rates, by contrast, directional locking results in deep local minima in D_L/D_0 at flow orientations slightly perturbed from 0°. Although the trends are qualitatively similar in systems with heterogeneous and homogeneous attractions, the magnitude of the changes in D_L/D_0 as θ or V_∞ is varied appears to be less pronounced in the heterogeneous systems. Hence, whereas attraction heterogeneity generally enhances dispersion, particularly at low flow rates, it appears to reduce the sensitivity of D_L/D_0 to variations in flow.

4. Conclusion

We examined the effects of heterogeneous attractive particle-medium interactions on transport in ordered nanopost arrays using SD simulations. Transport under quiescent conditions was found to be influenced by the interplay of mechanisms involving diffusion through the void space and intermittent hopping between the attractive wells of different nanoposts. As

the attraction heterogeneity increased, the latter mechanism became increasingly dominant, resulting in an increase in the particle trajectory tortuosity, deviations from Gaussian behavior in the particle displacement distributions, and a decrease in the long-time particle diffusivity. These behaviors are different from those observed in previous studies of structurally heterogeneous materials. Whereas non-Gaussian particle displacement distributions have also been reported in structurally disordered media, increasing structural heterogeneity creates large void spaces in the medium that enhance diffusion.[51]

Under flow conditions, transport was found to be strongly influenced by the interplay between thermal fluctuations, attractive particle–nanopost interactions, and advective drag forces. At low Pe, increased attraction heterogeneity led to transient localization near the nanoposts, resulting in a broadening of the particle distribution and enhanced longitudinal dispersion in the direction of flow. At high Pe where advection strongly dominates, however, the longitudinal dispersion coefficient was insensitive to attraction heterogeneity and exhibited approximately quadratic scaling with Pe, consistent with the Taylor–Aris model for dispersion *via* molecular diffusion.[12,78,87] By contrast, prior studies of tracer particles show that increasing structural heterogeneity in porous media results in mechanical dispersion becoming increasingly dominant and an associated crossover from quadratic to linear scaling with Pe in this regime.[86] Finally, we found that attraction heterogeneity does not strongly affect directional locking behavior. To our knowledge, the effects of structural disorder on directional locking have not been systematically studied, but due to the sensitivity of this behavior to flow orientation and lattice structure, we expect that it would be increasingly suppressed as structural heterogeneity increases. Interestingly, computational studies of flexible arrays have revealed that directional locking can be enhanced by local distortions that occur in response to interactions with transported particles.[17] Thus, this topic presents an interesting avenue for future investigation.

Conflicts of interest

There are no conflicts to declare.

Acknowledgements

Notes and references

1 B. W. J. Pirok, N. Abdulhussain, T. Aalbers, B. Wouters, R. A. H. Peters and P. J. Schoenmakers, *Anal. Chem.*, 2017, **89**, 9167–9174.

2 M. Zarei, M. Zarei and M. Ghasemabadi, *TrAC, Trends Anal. Chem.*, 2017, **86**, 56–74.

3 H. ShamsiJazeyi, C. A. Miller, M. S. Wong, J. M. Tour and R. Verduzco, *J. Appl. Polym. Sci.*, 2014, **131**, 40576.

4 M. Vallet-Regí, M. Colilla, I. Izquierdo-Barba and M. Manzano, *Molecules*, 2017, **23**, 47.

5 F.-Y. Kong, J.-W. Zhang, R.-F. Li, Z.-X. Wang, W.-J. Wang and W. Wang, *Molecules*, 2017, **22**, 1445.

6 C. Peng, J. Xu, M. Yu, X. Ning, Y. Huang, B. Du, E. Hernandez, P. Kapur, J.-T. Hsieh and J. Zheng, *Angew. Chem., Int. Ed.*, 2019, **58**, 8479–8483.

7 R. Chen, R. Poling-Skutvik, A. Nikoubashman, M. P. Howard, J. C. Conrad and J. C. Palmer, *Macromolecules*, 2018, **51**, 1865–1872.

8 R. Chen, R. Poling-Skutvik, M. P. Howard, A. Nikoubashman, S. A. Egorov, J. C. Conrad and J. C. Palmer, *Soft Matter*, 2019, **15**, 1260–1268.

9 R. C. Roberts, R. Poling-Skutvik, J. C. Palmer and J. C. Conrad, *J. Phys. Chem. Lett.*, 2018, **9**, 3008–3013.

10 R. Poling-Skutvik, R. C. Roberts, A. H. Slim, S. Narayanan, R. Krishnamoorti, J. C. Palmer and J. C. Conrad, *J. Phys. Chem. Lett.*, 2019, **10**, 1784–1789.

11 R. C. Roberts, R. Poling-Skutvik, J. C. Conrad and J. C. Palmer, *J. Chem. Phys.*, 2019, **151**, 194501.

12 D. L. Koch, R. G. Cox, H. Brenner and J. F. Brady, *J. Fluid Mech.*, 1989, **200**, 173–188.

13 J. P. Gleeson, J. M. Sancho, A. Lacasta and K. Lindenberg, *Phys. Rev. E: Stat., Nonlinear, Soft Matter Phys.*, 2006, **73**, 041102.

14 J. Herrmann, M. Karweit and G. Drazer, *Phys. Rev. E: Stat., Nonlinear, Soft Matter Phys.*, 2009, **79**, 061404.

15 R. J. Phillips, W. M. Deen and J. F. Brady, *AIChE J.*, 1989, **35**, 1761–1769.

16 R. J. Phillips, W. M. Deen and J. F. Brady, *J. Colloid Interface Sci.*, 1990, **139**, 363–373.

17 C. Reichhardt and C. O. Reichhardt, *Phys. Rev. E: Stat., Nonlinear, Soft Matter Phys.*, 2004, **69**, 041405.

18 C. Reichhardt, C. O. Reichhardt and M. Hastings, *Phys. Rev. E: Stat., Nonlinear, Soft Matter Phys.*, 2004, **69**, 056115.

19 K. Lindenberg, A. M. Lacasta, J. M. Sancho and A. Romero, *New J. Phys.*, 2005, **7**, 29.

20 A. M. Lacasta Palacio, J. M. Sancho, A. Romero and K. Lindenberg, *Phys. Rev. Lett.*, 2005, **94**, 160601.

21 A. Lacasta, M. Khoury, J. M. Sancho and K. Lindenberg, *Mod. Phys. Lett. B*, 2006, **20**, 1427–1442.

22 K. Lindenberg, J. M. Sancho, A. Lacasta and I. M. Sokolov, *Phys. Rev. Lett.*, 2007, **98**, 020602.

23 J. Frechette and G. Drazer, *J. Fluid Mech.*, 2009, **627**, 379–401.

24 C. Reichhardt and C. O. Reichhardt, *Phys. Rev. Lett.*, 2011, **106**, 060603.

25 D. Hlushkou, F. Gritti, A. Daneyko, G. Guiochon and U. Tallarek, *J. Phys. Chem. C*, 2013, **117**, 22974–22985.

26 D. Hlushkou, F. Gritti, G. Guiochon, A. Seidel-Morgenstern and U. Tallarek, *Anal. Chem.*, 2014, **86**, 4463–4470.

27 J. Hansing and R. R. Netz, *Macromolecules*, 2018, **51**, 7608–7620.

28 D. L. Koch and J. F. Brady, *J. Fluid Mech.*, 1985, **154**, 399–427.

29 J. Salles, J. F. Thovert, R. Delannay, L. Prevors, J. L. Auriault and P. M. Adler, *Phys. Fluids A*, 1993, **5**, 2348–2376.

30 R. S. Maier, D. M. Kroll, R. S. Bernard, S. E. Howington, J. F. Peters and H. T. Davis, *Phys. Fluids*, 2000, **12**, 2065–2079.

31 D. Edwards, M. Shapiro, H. Brenner and M. Shapira, *Transp. Porous Media*, 1991, **6**, 337–358.

32 H. P. A. Souto and C. Moyne, *Phys. Fluids*, 1997, **9**, 2253–2263.

33 S. Sirivithayapakorn and A. Keller, *Water Resour. Res.*, 2003, **39**, 1109.

34 T. Stylianopoulos, B. Diop-Frimpong, L. L. Munn and R. K. Jain, *Biophys. J.*, 2010, **99**, 3119–3128.

35 D. Mangal, J. C. Conrad and J. C. Palmer, *AIChE J.*, 2021, **67**, e17147.

36 P. Bacchin, A. Marty, P. Duru, M. Meireles and P. Aimar, *Adv. Colloid Interface Sci.*, 2011, **164**, 2–11.

37 T. Zhang, M. J. Murphy, H. Yu, H. G. Bagaria, K. Y. Yoon, B. M. Neilson, C. W. Bielawski, K. P. Johnston, C. Huh and S. L. Bryant, *SPE J.*, 2015, **20**, 667–677.

38 C. V. Chrysikopoulos, P. K. Kitanidis and P. V. Roberts, *Transp. Porous Media*, 1992, **7**, 163–185.

39 X. Yan, Q. Wang and H. H. Bau, *J. Chromatogr. A*, 2010, **1217**, 1332–1342.

40 L. Li, X. Yan, J. Yang and Q. Wang, *Appl. Energy*, 2017, **185**, 2168–2180.

41 T. Stylianopoulos, M.-Z. Poh, N. Insin, M. G. Bawendi, D. Fukumura, L. L. Munn and R. K. Jain, *Biophys. J.*, 2010, **99**, 1342–1349.

42 D. Mangal, J. C. Conrad and J. C. Palmer, *Phys. Rev. E*, 2022, **105**, 055102.

43 Y. Bernabé and C. Bruderer, *J. Geophys. Res.: Solid Earth*, 1998, **103**, 513–525.

44 M. Auset and A. A. Keller, *Water Resour. Res.*, 2004, **40**, W03503.

45 H. F. Lecoanet, J.-Y. Bottero and M. R. Wiesner, *Environ. Sci. Technol.*, 2004, **38**, 5164–5169.

46 J. C. Palmer, J. D. Moore, J. K. Brennan and K. E. Gubbins, *Adsorption*, 2011, **17**, 189–199.

47 S. Sasidharan, S. Torkzaban, S. A. Bradford, P. J. Dillon and P. G. Cook, *Colloids Surf., A*, 2014, **457**, 169–179.

48 J. D. C. Jacob, R. Krishnamoorti and J. C. Conrad, *Phys. Rev. E*, 2017, **96**, 022610.

49 S. Aramideh, P. P. Vlachos and A. M. Ardekani, *J. Non-Newtonian Fluid Mech.*, 2019, **268**, 75–80.

50 D. M. Walkama, N. Waisbord and J. S. Guasto, *Phys. Rev. Lett.*, 2020, **124**, 164501.

51 I. Chakraborty and Y. Roichman, *Phys. Rev. Res.*, 2020, **2**, 022020.

52 A. Pacheco-Pozo and I. M. Sokolov, *Phys. Rev. Lett.*, 2021, **127**, 120601.

53 R. Pastore, A. Ciarlo, G. Pesce, A. Sasso and F. Greco, *Soft Matter*, 2022, **18**, 351–364.

54 T. Shende, D. Mangal, J. C. Conrad, V. Niasar and M. Babaei, *Phys. Rev. E*, 2022, **106**, 015103.

55 J. A. L. Kemps and S. Bhattacharjee, *Langmuir*, 2005, **21**, 11710–11721.

56 T. R. Kline, G. Chen and S. L. Walker, *Langmuir*, 2008, **24**, 9381–9385.

57 B. Mustin and B. Stoeber, *Langmuir*, 2016, **32**, 88–101.

58 P. R. Johnson, N. Sun and M. Elimelech, *Environ. Sci. Technol.*, 1996, **30**, 3284–3293.

59 N. Tufenkji and M. Elimelech, *Langmuir*, 2004, **20**, 10818–10828.

60 S. A. Bradford and S. Torkzaban, *Langmuir*, 2012, **28**, 13643–13651.

61 S. A. Bradford and S. Torkzaban, *Langmuir*, 2013, **29**, 3668–3676.

62 R. P. Jaiswal and S. P. Beaudoin, *Langmuir*, 2019, **35**, 86–94.

63 M. Zhang, S. A. Bradford, J. Šimunek, H. Vereecken and E. Klumpp, *Environ. Pollut.*, 2019, **247**, 907–916.

64 C. Shen, Y. Jin, J. Zhuang, T. Li and B. Xing, *Crit. Rev. Environ. Sci. Technol.*, 2020, **50**, 244–329.

65 W. J. C. Holt and D. Y. C. Chan, *Langmuir*, 1997, **13**, 1577–1586.

66 M. Bendersky and J. M. Davis, *J. Colloid Interface Sci.*, 2011, **353**, 87–97.

67 C. Shen, V. Lazouskaya, H. Zhang, B. Li, Y. Jin and Y. Huang, *Colloids Surf., A*, 2013, **433**, 14–29.

68 R. D. Duffadar and J. M. Davis, *J. Colloid Interface Sci.*, 2007, **308**, 20–29.

69 Y. Li, A. Ahmadi, A. Omari and H. Pu, *Colloids Surf., A*, 2020, **586**, 124166.

70 L. R. Huang, E. C. Cox, R. H. Austin and J. C. Sturm, *Science*, 2004, **304**, 987–990.

71 J. McGrath, M. Jimenez and H. Bridle, *Lab Chip*, 2014, **14**, 4139–4158.

72 S. Du, S. Shojaei-Zadeh and G. Drazer, *Soft Matter*, 2017, **13**, 7649–7656.

73 L. K. Månsson, T. de Wild, F. Peng, S. H. Holm, J. O. Tegenfeldt and P. Schurtenberger, *Soft Matter*, 2019, **15**, 8512–8524.

74 L. Zhu, C. Rorai, D. Mitra and L. Brandt, *Soft Matter*, 2014, **10**, 7705–7711.

75 J. O. de Beeck, W. D. Malsche, P. D. Moor and G. Desmet, *J. Sep. Sci.*, 2012, **35**, 1877–1883.

76 A. Daneyko, D. Hlushkou, S. Khirevich and U. Tallarek, *J. Chromatogr. A*, 2012, **1257**, 98–115.

77 A. M. Striegel and A. K. Brewer, *Annu. Rev. Anal. Chem.*, 2012, **5**, 15–34.

78 D. Mangal, J. C. Palmer and J. C. Conrad, *Phys. Rev. E*, 2021, **104**, 015102.

79 F. Babayekhorasani, D. E. Dunstan, R. Krishnamoorti and J. C. Conrad, *Soft Matter*, 2016, **12**, 8407–8416.

80 J. F. Brady and G. Bossis, *Annu. Rev. Fluid Mech.*, 1988, **20**, 111–157.

81 R. J. Phillips, J. F. Brady and G. Bossis, *Phys. Fluids*, 1988, **31**, 3473–3479.

82 M. Wang and J. F. Brady, *J. Chem. Phys.*, 2015, **142**, 094901.

83 M. P. Howard, A. Gautam, A. Z. Panagiotopoulos and A. Nikoubashman, *Phys. Rev. Fluids*, 2016, **1**, 044203.

84 R. J. Phillips, *Biophys. J.*, 2000, **79**, 3350.

85 J. Hansing, C. Ciemer, W. K. Kim, X. Zhang, J. E. DeRouchey and R. R. Netz, *Eur. Phys. J. E: Soft Matter Biol. Phys.*, 2016, **39**, 1–13.

86 C. Bruderer and Y. Bernabé, *Water Resour. Res.*, 2001, **37**, 897–908.

87 R. Aris, *Proc. R. Soc. London, Ser. A*, 1956, **235**, 67–77.

88 W. Chien and Y.-L. Chen, *Soft Matter*, 2016, **12**, 7969–7976.

89 P. Linse and N. Kallrot, *Macromolecules*, 2010, **43**, 2054–2068.

90 J. Frenkel, *Kinetic theory of liquids*, Dover Publications, 1955.

91 A. Felinger, *J. Chromatogr. A*, 2008, **1184**, 20–41.

92 J. Koplik and G. Drazer, *Phys. Fluids*, 2010, **22**, 052005.